

See discussions, stats, and author profiles for this publication at: <https://www.researchgate.net/publication/259287498>

Higher Order Amyloid Fibril Structure by MAS NMR and DNP Spectroscopy

DATASET · DECEMBER 2013

CITATION

1

READS

30

14 AUTHORS, INCLUDING:



[Anthony William Paul Fitzpatrick](#)

University of Cambridge

12 PUBLICATIONS 633 CITATIONS

[SEE PROFILE](#)



[Vladimir Ladizhansky](#)

University of Guelph

61 PUBLICATIONS 1,619 CITATIONS

[SEE PROFILE](#)



[Christopher P Jaroniec](#)

The Ohio State University

68 PUBLICATIONS 3,427 CITATIONS

[SEE PROFILE](#)



[Michele Vendruscolo](#)

University of Cambridge

349 PUBLICATIONS 12,669 CITATIONS

[SEE PROFILE](#)

Higher Order Amyloid Fibril Structure by MAS NMR and DNP Spectroscopy

Galia T. Debelouchina,^{†,||} Marvin J. Bayro,^{†,■} Anthony W. Fitzpatrick,^{‡,●} Vladimir Ladizhansky,^{†,▼} Michael T. Colvin,[†] Marc A. Caporini,^{‡,§} Christopher P. Jaroniec,^{†,◆} Vikram S. Bajaj,^{†,▽} Melanie Rosay,[§] Cait E. MacPhee,[⊥] Michele Vendruscolo,[‡] Werner E. Maas,[§] Christopher M. Dobson,[‡] and Robert G. Griffin^{*,†}

[†]Francis Bitter Magnet Laboratory and Department of Chemistry, Massachusetts Institute of Technology, Cambridge, Massachusetts 02139, United States

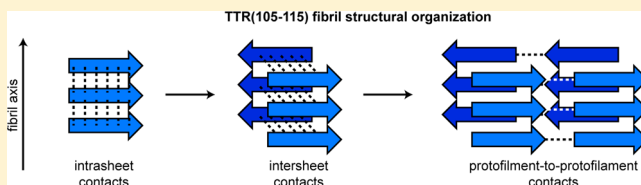
[‡]Department of Chemistry, University of Cambridge, Cambridge CB2 1EW, United Kingdom

[§]Bruker BioSpin Corporation, Billerica, Massachusetts 01821, United States

[⊥]James Clerk Maxwell Building, School of Physics, University of Edinburgh, The Kings Buildings, Mayfield Road, Edinburgh EH9 3JZ, United Kingdom

Supporting Information

ABSTRACT: Protein magic angle spinning (MAS) NMR spectroscopy has generated structural models of several amyloid fibril systems, thus providing valuable information regarding the forces and interactions that confer the extraordinary stability of the amyloid architecture. Despite these advances, however, obtaining atomic resolution information describing the higher levels of structural organization within the fibrils remains a significant challenge. Here, we detail MAS NMR experiments and sample labeling schemes designed specifically to probe such higher order amyloid structure, and we have applied them to the fibrils formed by an eleven-residue segment of the amyloidogenic protein transthyretin (TTR(105–115)). These experiments have allowed us to define unambiguously not only the arrangement of the peptide β -strands into β -sheets but also the β -sheet interfaces within each protofilament, and in addition to identify the nature of the protofilament-to-protofilament contacts that lead to the formation of the complete fibril. Our efforts have resulted in 111 quantitative distance and torsion angle restraints (10 per residue) that describe the various levels of structure organization. The experiments benefited extensively from the use of dynamic nuclear polarization (DNP), which in some cases allowed us to shorten the data acquisition time from days to hours and to improve significantly the signal-to-noise ratios of the spectra. The β -sheet interface and protofilament interactions identified here revealed local variations in the structure that result in multiple peaks for the exposed N- and C-termini of the peptide and in inhomogeneous line-broadening for the residues buried within the interior of the fibrils.



INTRODUCTION

The deposition of amyloid fibrils in tissues and cells is the characteristic feature of more than 25 different human pathologies,¹ and amyloid fibrils with functional roles have been identified in several species, including humans.^{1,2} In addition, many proteins and peptides can readily form amyloid fibrils in vitro typically under non-native conditions such as low pH, high salt concentration, or the presence of metal ions.³ While the proteins and peptides that have been reported to form amyloid structures are very diverse in their sequences and native folds, the resulting fibrils share several physicochemical characteristics: they are rich in β -sheet structure; they bind the dye Congo red, resulting in a green birefringence under polarized light; and they yield a distinctive “cross- β ”^{4,5} X-ray diffraction pattern. This pattern consists of two reflections, one indicative of a 4.7 Å separation between the β -strands along the fibril axis, and a second corresponding to an 8–11 Å distance,

which results from the sheet-to-sheet separation perpendicular to the fibril axis.

The development of MAS NMR experiments applicable to proteins has contributed significantly to the understanding of amyloid fibril structure and the underlying forces that lead to the formation of these insoluble, noncrystalline protein assemblies.⁶ To date, progress has been made in the NMR structural studies of amyloid fibrils formed by many peptides and proteins including $A\beta$,^{7–9} HET-s,^{10,11} α -synuclein,^{12–14} β_2 -microglobulin,^{15,16} the SH3 domain of PI3 kinase,^{17,18} and the human prion protein.^{19,20} These studies have provided valuable information regarding the location of the β -strands within the polypeptide sequence, the arrangement of the β -strands into β -sheets, and in some cases the organization of the β -sheets into the fibril protofilaments. Cryo-electron microscopy (cryo-EM)

Received: September 1, 2013

and atomic force microscopy (AFM), on the other hand, have revealed the remarkable structural complexity of amyloid fibrils, often manifest as distinct fibril forms sometimes organized into elaborate structures containing features such as “hollow” cores, “fuzzy coats” or stacks of globular domains.^{21–25} While the combination of MAS NMR on one hand, and cryo-EM and AFM on the other, can be a very powerful approach in amyloid fibril structure determination, many challenges exist in bridging the gap between the atomic resolution structural information afforded by NMR and the electron density maps generated by approaches like cryo-EM. In particular, the interactions that mediate the formation of the protofilament-to-protofilament interfaces and contribute to the extraordinary stability of amyloid fibrils have remained particularly elusive.

Here, we focus on the fibrils formed by a small segment (residues 105–115) of the protein transthyretin (TTR), associated with familial amyloid polyneuropathy and senile systemic amyloidosis.^{26,27} This segment participates in interactions involved in the stabilization of the homotetramer architecture of functional TTR and may play an important role in the amyloidogenesis of the protein. On its own, TTR(105–115) is amyloidogenic at low pH, and the structure of the peptide monomer was one of the initial structures of biologically relevant molecules determined *de novo* by MAS NMR and the first atomic resolution structure of a molecule within an amyloid fibril (Figure 1).^{28,29} Based on 76 structurally

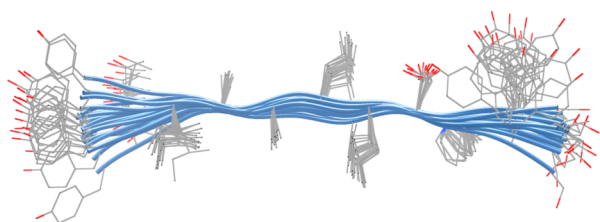


Figure 1. Structure of the TTR(105–115) monomer in amyloid fibrils (PDB ID: 1RVS).²⁹ The ensemble of 20 lowest energy structures is depicted.

relevant constraints (7 per residue), this structure established that the peptide in the fibril form adopts an extended β -strand conformation with no significant dynamic behavior within the backbone of the molecule. The structure analysis relied on the use of three U-¹⁵N, ¹³C samples where only four residues were concurrently labeled (YTIAALLSPYS, YTIAALLSPYS, YTIAALLSPYS), thus allowing the unambiguous assignment of the chemical shifts, and the measurement of intramolecular distances and ϕ and ψ backbone torsion angles.

Recently, we combined MAS NMR, cryo-EM, AFM, and scanning transmission electron microscopy (STEM) experiments to determine at atomic resolution the higher order structural organization of the TTR(105–115) peptide into three amyloid polymorphs (PDB IDs: 2m5k, 2m5m, 2m5n).³⁰ These structures reveal that the peptide molecules are aligned into parallel, in-register β -sheets; the β -sheets are arranged in an antiparallel fashion with respect to each other and thus define each individual protofilament in the assembly. The mature fibrils contain four, six, or eight protofilaments, assembled laterally in two layers separated by a 13 Å region of low density. The protofilaments are stabilized by extensive backbone-to-backbone hydrogen bonds along the length of each β -sheet and have a dry, hydrophobic interface between the antiparallel β -sheets. The protofilament-to-protofilament contacts, on the

other hand, result from staggered hydrogen bonds and electrostatic interactions between the terminal C=O and N–H groups of the peptides in a pair of adjacent protofilaments.

In this work, we present and evaluate the complete suite of MAS NMR experiments and labeling schemes that have allowed us to characterize the different levels of structural organization in the TTR(105–115) fibrils described in ref 30. As there are many possible structural states accessible to small peptides in the amyloid form,³¹ we focus specifically on strategies designed to identify and assign unambiguously and efficiently the relevant structural interactions within the hierarchical assembly of the fibrils. We show how dynamic nuclear polarization^{32–39} (DNP), a method that significantly improves the sensitivity of MAS NMR experiments, can be integrated into the structure determination protocol and used to generate precise distance constraints much more efficiently. In addition, we provide experimental evidence for the existence of local structural variations in the TTR(105–115) fibrils that are consistent with the proposed structure and that contribute to peak multiplicity and inhomogeneous line-broadening in the NMR spectra.

RESULTS AND DISCUSSION

DNP of TTR(105–115) Fibrils. DNP utilizes the inherently larger polarization of electrons, which is transferred to the nuclei via a microwave-driven process performed at low temperatures (90–100 K). The electrons are introduced to the sample in the form of a biradical, typically TOTAPOL,⁴⁰ and glycerol is added for cryoprotection. The significant signal enhancements demonstrated in MAS DNP experiments have been utilized in the study of a variety of biological systems, including membrane proteins,^{41–46} nanocrystals,^{47,48} cellular components,^{49,50} and amyloid fibrils.^{18,48} In particular, studies of the fibrils formed by the GNNQQNY peptide⁴⁸ demonstrate that the sample integrity and structure is preserved in the DNP samples and that the low temperatures utilized in DNP experiments suppress dynamic processes that can interfere with the recoupling experiment of choice, in this case ZF-TEDOR.⁵¹ Subsequently, DNP-enhanced ZF-TEDOR was used to show that the fibrils formed by the SH3 domain of PI3 kinase form parallel, in-register β -sheets.¹⁸ The enhancement factor of ~30 and the diminished influence of dynamics on the dipolar transfer, particularly for the side chains, allowed the collection of a much greater set of intermolecular structural constraints in a fraction of the conventional experimental time. Here, we use DNP-enhanced MAS NMR spectroscopy to obtain quantitative structural constraints for the TTR(105–115) fibrils.

Figure 2 shows the DNP-enhanced ¹³C CP spectrum of TTR(105–115) fibrils labeled with ¹³C at the S115 carbonyl atom. A modest DNP enhancement of ~11 was observed in this fibril sample prepared with 10 mM TOTAPOL in a 60/40% w/w glycerol-*d*₈/buffer matrix, where the buffer consisted of a 10/90% v/v acetonitrile/D₂O mixture with pD adjusted to 2.0 with HCl. The polarization buildup time was 1.3 s, which correlates with the ¹H *T*₁,⁴⁰ and allowed us to record experiments with a 2.0 s recycle delay. Both the enhancement factor and the buildup time in this fibril system are lower than the numbers reported for the GNNQQNY fibrils (ϵ = 35, buildup time 5 s)⁴⁸ and PI3 SH3 fibrils (ϵ = 30, buildup time 3.5 s),¹⁸ obtained using an identical DNP spectrometer and TOTAPOL concentration. These differences can be due to a variety of factors: the buffer composition and pH can affect the stability of the TOTAPOL radical, while the ¹H *T*₁, and hence

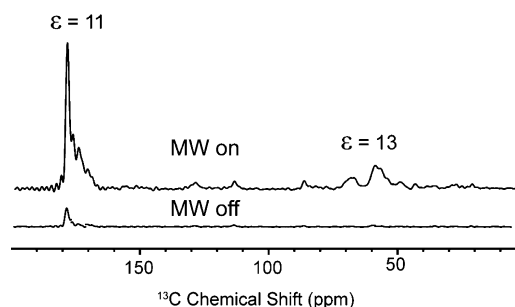


Figure 2. DNP-enhanced ^{13}C CP spectrum of TTR(105–115) fibrils labeled with ^{13}C at the S115 carbonyl atom (top). An additional spectrum was recorded under identical experimental conditions but without microwave irradiation (bottom) in order to determine the enhancement due to DNP. The enhancement for the labeled carbonyl atom was 11, while the enhancement for the natural abundance signals in the sample was 13. Spectra were recorded on a spectrometer operating at 400 MHz ^1H Larmor frequency.

the enhancement, are very sensitive to overall protonation levels within the sample and slight differences in the effective temperature during the experiment. In the TTR(105–115) case, in particular, the presence of multiple methyl groups in the peptide itself, and in the acetonitrile used in the buffer matrix, provide additional relaxation sinks. Nevertheless, the relatively short T_1 in the TTR(105–115) sample allowed us to record quantitative DQ-DRAWS build-up and REDOR dephasing curves (see below) in one to two hours compared to days for the standard room-temperature experiments.

Intrasheet Arrangement. Once the secondary structure of the monomer in the fibrils is known (Figure 1), the next step of the structure determination process involves establishing the organization of the β -strands into β -sheets. The parallel, in-register arrangement is quite common among amyloid fibrils formed by large peptides (longer than 20 residues)^{52–54} and proteins,^{16,18,20,55} although the more complicated arrangement where one molecule forms two loops of a β -helix, and thus participates with two β -strands in a parallel β -sheet, has also been described.¹⁰ In the case of small amyloidogenic peptides, both parallel and antiparallel arrangements have been observed in crystals,³¹ with the strands being in-register or out-of-register with an arbitrary residue offset (Figure 3a).

Several approaches exist for unraveling the intrasheet arrangement of β -strands in amyloid fibrils. In longer peptides and proteins, a common method involves preparing fibril samples from a 50/50 mixture of exclusively ^{13}C and exclusively ^{15}N labeled monomers and examining the nature of the intermolecular correlations in the ^{15}N – ^{13}C spectra.^{11,16,18,20,54} This strategy requires the use of long mixing times to probe ^{15}N – ^{13}C distances on the order of 4–5 Å, and the acquisition times can sometimes be prohibitively long. It has recently been shown, however, that DNP can be successfully combined with this approach to yield a large number of additional intrasheet constraints.¹⁸ Information regarding the intrasheet organization can also be obtained from more sensitive long-mixing 2D ^{13}C – ^{13}C correlation experiments of samples prepared with 2- ^{13}C glycerol as the carbon source.¹⁸ In shorter peptides, where many possibilities exist for the supramolecular arrangement of the peptides in the fibril,⁵⁶ the structure determination can be simplified by the use of specific labeling, and symmetry-based⁵⁷ or double quantum pulse sequences^{58,59} have been used to obtain the corresponding distances and arrangements.

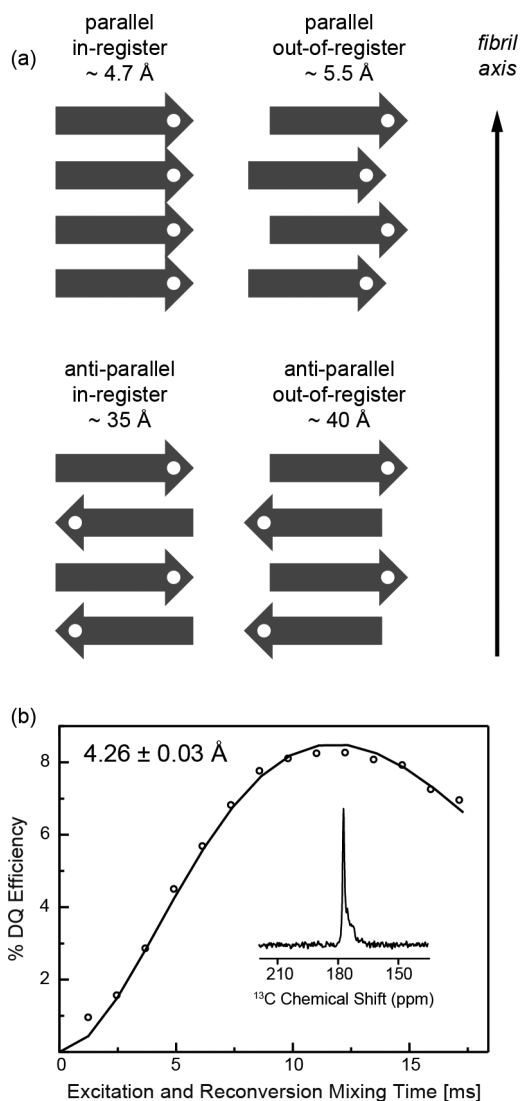


Figure 3. (a) Several possible arrangements of the β -strands within each sheet, along with the expected distances between labeled carbonyl atoms (white circles). (b) DNP-enhanced DQF-DRAWS experiment obtained at 400 MHz (^1H Larmor frequency) with a sample labeled with ^{13}C at the S115 carbonyl position. The fit distance is 4.26 ± 0.03 Å, consistent with a parallel, in-register intrasheet arrangement. The inset shows the 1D DQF-DRAWS spectrum obtained with $\tau_{\text{mix}} = 12.2$ ms to illustrate the sensitivity of the DNP-enhanced experiment. All 14 mixing points were recorded in ~ 1.5 h total.

For our studies of TTR(105–115), eight different samples were prepared where each sample was labeled only at the carbonyl position for each one of the residues I107–P113 and S115.^{30,60} The possible intrasheet distances for the carbonyl atom of the S115 residue are illustrated in Figure 3a. In the parallel, in-register case, the labeled atoms form an infinite chain of spins where all the nuclei have identical chemical shifts and are separated by ~ 4.7 Å. When the two strands in the β -sheet are parallel but one residue out-of-register, a “zig-zag” pattern emerges with expected average distances of ~ 5.5 Å. In the antiparallel case, the expected distances for most of the single-labeled TTR(105–115) samples are too long to measure with ^{13}C – ^{13}C dipolar recoupling techniques. Double-quantum filtered DRAWS (DQF-DRAWS) is particularly well-suited to explore the possible strand arrangements, as it can yield very precise distances for spins with degenerate chemical shifts and

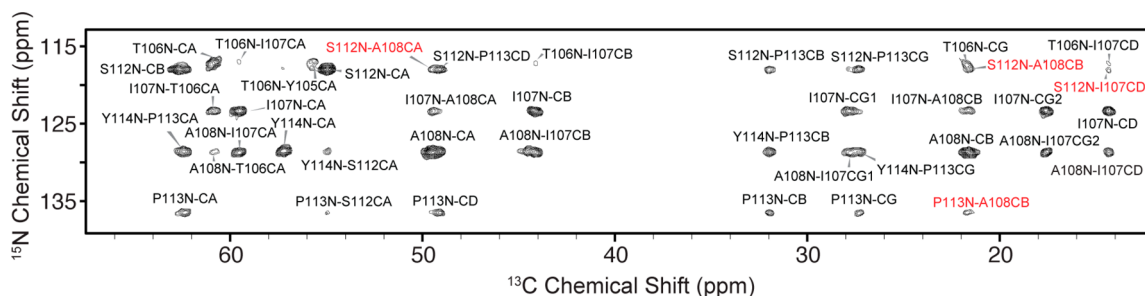


Figure 4. PAIN-CP ^{15}N - ^{13}C correlation experiment used in defining the intersheet organization of the TTR(105–115) fibrils. The spectrum was obtained at a ^1H Larmor frequency of 900 MHz with $\tau_{\text{mix}} = 10$ ms and a U- ^{13}C , ^{15}N YTIAALLSPYS-labeled TTR(105–115) fibril sample. Intersheet correlations are labeled in red, and intrasheet contributions are shown in black.

large chemical shift anisotropies such as those present in carbonyl and carboxyl groups.^{59–61}

The DQF-DRAWS experiments for the eight singly labeled TTR(105–115) samples revealed carbonyl-to-carbonyl distances in the range of 4.3–4.6 Å, as described in refs 30 and 60. These distances are consistent with a parallel, in-register arrangement of the β -strands in the fibrils. Here, we present the DNP-enhanced 1D DQF-DRAWS buildup curve for the $^{13}\text{C}_1$ S115 sample (shown in Figure 3b), with a maximum DQ efficiency of $\sim 8\%$, occurring at $\tau_{\text{mix}} \approx 12$ ms. The curve through the experimental data was simulated with the program SPINEVOLUTION,⁶² using a four-spin model with a boundary condition to account for the infinite chain of nuclear spins, and a relaxation parameter that models the effects of incoherent relaxation and experimental imperfections.⁶⁰ The intermolecular distance measured with DNP is 4.26 ± 0.03 Å, in excellent agreement with the distance recorded at room temperature (4.29 ± 0.05 Å). The DNP-enhanced buildup curve was recorded in only 1.5 h, while the equivalent experiment at room temperature without DNP required 3.5 days of acquisition time. For eight samples, the total acquisition time thus could be shortened from several weeks to approximately one day.

Intersheet Contacts. Much of what is known about the intersheet interfaces in amyloid fibrils, particularly those formed by small peptides, is derived from the X-ray structures of microcrystals formed by amyloidogenic peptides.^{31,56} In such crystals, the intersheet interface is free of water molecules, and the side chains of the adjacent sheets are tightly interdigitated, forming the so-called steric zipper. A wet interface then may exist on the outside surfaces of the β -sheets for some peptides. On the basis of the crystal structures of thirteen different peptides, eight possible different classes of steric zippers were proposed, some of them yet to be observed experimentally.³¹ While this information is extremely valuable in understanding the interactions that stabilize amyloid structures, it is only part of the story for some peptides. For example, GNNQQNY, a short segment from the yeast prion protein Sup35, can form both monoclinic and orthorhombic crystals and also fibrils at different peptide concentrations. MAS NMR spectra of both crystal forms revealed different sets of chemical shifts and those of the fibrils showed three sets of chemical shifts, all different from those observed from either crystal, respectively.^{63,64} Similar structural complexity has been observed for the fibrils formed by the peptide SNNFGAILSS, related to type 2 diabetes.⁶⁵

In order to address this potential problem for TTR(105–115), we prepared two specifically labeled samples, **YTIAALL-SPYS** and **YTIAALLSPYS** (uniformly ^{15}N , ^{13}C -labeled at the

bold-faced residues), that allowed us to characterize the intersheet contacts throughout the length of the peptide. Previously, we have shown PDSD⁶⁶ spectra recorded with the **YTIAALLSPYS** sample (see ref 30 and Figure S1 for a representative example). Even at relatively short mixing times, there are many cross peaks (Figure S1) in the spectra that correspond to correlations between residues at the opposite ends of the molecule (e.g., P113C β –A108C β and S112C α –I107C δ). Since the peptide molecules are organized in a parallel, in-register manner within the sheet, such correlations can only arise if the two sheets are arranged in an antiparallel fashion. Here, we present additional ¹⁵N–¹³C contacts in spectra recorded with PAIN-CP mixing^{67,68} (Figure 4 and Figure S2), where three intersheet backbone-to-side-chain correlations are observed (S112N–A108C β , S112N–I107C δ , P113N–A108C β), as well as one backbone-to-backbone correlation (S112N–A108C α). At longer mixing times, a correlation between I107N and P113C β is also observed (Figure S2).

Although the PDS and PAIN-CP data provide a very clear qualitative picture of the sheet-to-sheet interface in the fibrils and significant progress has been made in quantifying such correlations,⁶⁹ extracting distance information from such data sets remains a challenge. In the PDS case, for example, multiple spin diffusion pathways and relay transfer can complicate the distance interpretation. The PAIN-CP experiments, on the other hand, rely on a second-order recoupling mechanism involving a cross-term between ^1H – ^{15}N and ^1H – ^{13}C dipolar couplings, and so the intensity of the transfer has a strong geometric dependence on the position of the ^1H spin.⁶⁸ Therefore, the observed contacts in these type of spectra are usually separated in distance bins based on the mixing times when they are first observed. These rather broad distance classes are then used in the structure calculation, much like NOE constraints are used in solution NMR.

In order to complement the constraints from the PDS and PAIN-CP spectra, we performed 3D ZF-TEDOR experiments^{51,70} that allowed us to obtain accurate intersheet distances for P113N-A108C β , S112N-A108C β , and S112N-I107C δ 1 that were essential in the structure calculation process. The experiments consisted of recording 2D ^{15}N - ^{13}C correlations at different mixing times, then extracting the intensity of the cross peaks of interest and simulating the experimental build-up curves with SPINEVOLUTION (Figure 5). For comparison, Figure 5 also contains simulations of several known intramolecular distances in the TTR(105-115) molecule²⁹ that served as a validation of the simulation procedure. In particular, the TEDOR transfer dynamics

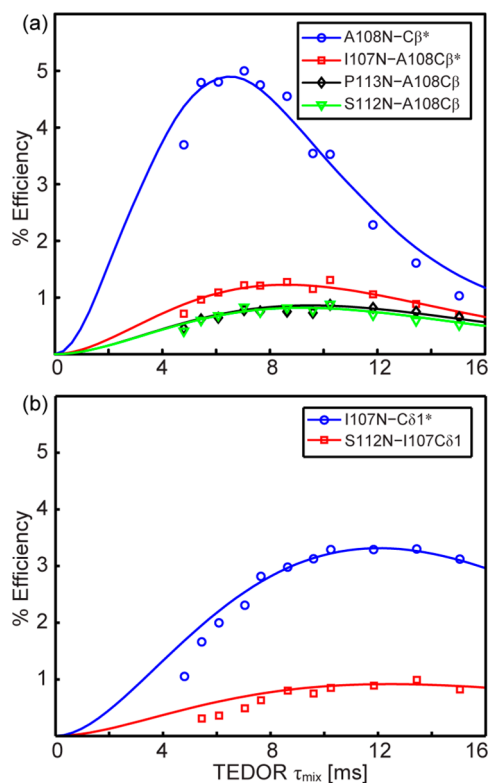


Figure 5. Experimental and simulated TEDOR buildup curves obtained from the cross-peak intensities in 2D ZF-TEDOR experiments recorded as a function of mixing time for (a) correlations to A108C β , and (b) correlations to I107C δ 1. The fitted distances are: 2.4 ± 0.2 Å for A108N-C β *, 4.8 ± 0.4 Å for I107N-A108C β *, 5.4 ± 0.5 Å for S112N-A108C β , 6.0 ± 0.4 Å for P113N-A108C β ; 4.3 ± 0.5 Å for I107N-C δ 1*, and 5.8 ± 0.5 Å for S112N-I107C δ 1. The intramolecular distances marked with asterisks are known (ref 29) and were used as a validation of the simulation procedure. Data were recorded at 750 MHz ^1H Larmor frequency.

between distal ^{15}N – ^{13}C pairs are influenced by the proximity of other ^{15}N atoms to the ^{13}C atom of interest. If such ^{15}N atoms are present nearby, the transfer from the distal ^{15}N atom can still be observed as a crosspeak in the 2D spectrum; however, it may occur on an accelerated time scale compared to the transfer for a lone ^{15}N – ^{13}C pair at an equivalent distance. For example, the I107N–A108C β distance (4.8 ± 0.4 Å) is longer than the I107N–C δ 1 distance (4.3 ± 0.5 Å), but the maxima of the two curves are at 9 and 12 ms, respectively. The transfer dynamics in the first case are accelerated due to the presence of A108N, which is only 2.4 Å away from the C β atom. In order to reflect the properties of the spin systems in relation to TEDOR transfer, we included the contribution of the proximal A108N atom in the simulations of the buildup curves involving A108C β (Figure 5a). A single ^{15}N atom was, however, sufficient to describe the TEDOR transfer when fitting the I107N–C δ 1 and S112N–I107C δ 1 distances (Figure 5b).

The distance constraints obtained from the YTIALLSPYS sample were complemented with distances measured with a sample uniformly ^{15}N and ^{13}C labeled in the center of the peptide molecule (i.e., YTIALLSPYS). Using the TEDOR experiment described above, cross peaks between A109N and L111C δ 1 and C δ 2 were observed with fitted distances of 4.4 ± 0.5 Å and 4.6 ± 0.5 Å, respectively (Figure 6a). With this sample, it was also possible to measure several long-distance

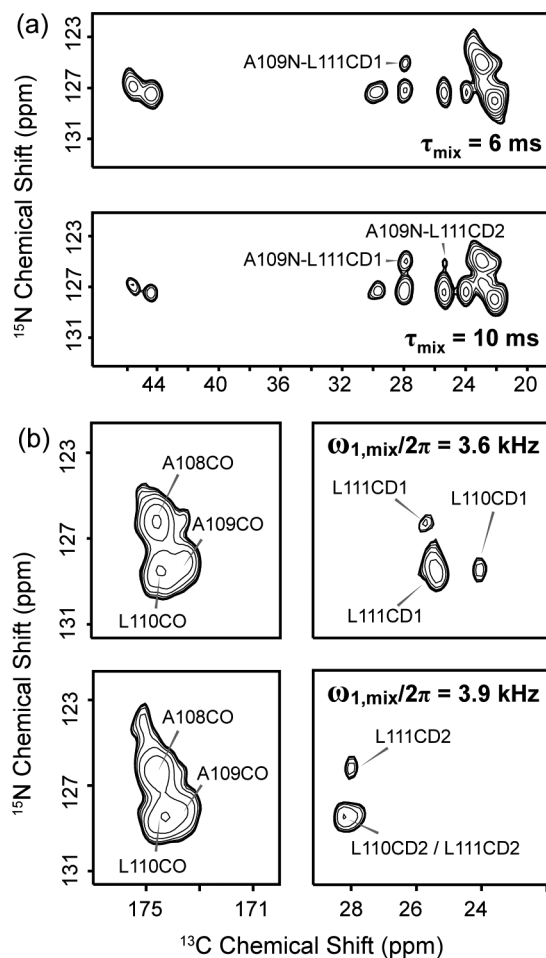


Figure 6. Two-dimensional ^{15}N – ^{13}C correlation spectra recorded at a ^1H Larmor frequency of 500 MHz with a YTIALLSPYS-labeled sample using (a) TEDOR mixing and (b) a rotational resonance in the tilted frame width (R^2TRW) experiment. Both spectra were recorded at a 10.1 kHz spinning rate and with the carrier frequency set at 65 ppm. The R^2TRW mixing time was 25 ms with 83 kHz TPPM decoupling during mixing. Examples of two ^{13}C recoupling fields used during the mixing period of the R^2TRW experiment are given in (b).

^{13}C – ^{13}C constraints that complemented the intersheet ^{15}N – ^{13}C distances acquired with TEDOR. Obtaining accurate long-range ^{13}C – ^{13}C distances in uniformly labeled samples can be quite challenging due to a phenomenon known as dipolar truncation.⁷¹ In this case, the strong one- and two-bond ^{13}C – ^{13}C couplings dominate the polarization transfer and the transfer to more distant carbon atoms is attenuated or eliminated. Experiments such as PDSD⁶⁶ and PAR⁷² are less sensitive to these effects since they rely on higher-order mechanisms; however, as discussed above, they yield only semiquantitative distance restraints due to the complexity of the polarization transfer.

To obtain accurate ^{13}C – ^{13}C distances in the YTIALLSPYS-labeled peptide, we used the rotational resonance in the tilted frame width experiment⁷³ (R^2TRW) to reintroduce the ^{13}CO – $^{13}\text{C}\gamma,\delta$ dipolar interactions without reintroducing the strong ^{13}CO – $^{13}\text{C}\alpha$ or ^{13}CO – $^{13}\text{C}\beta$ couplings, thus avoiding dipolar truncation. The experiment starts with ^1H – ^{15}N cross polarization,⁷⁴ t_1 evolution of the ^{15}N dimension, and selective transfer of polarization from ^{15}N to the labeled carbonyls in the sample via SPECIFIC CP.⁷⁵ The inclusion of a ^{15}N dimension

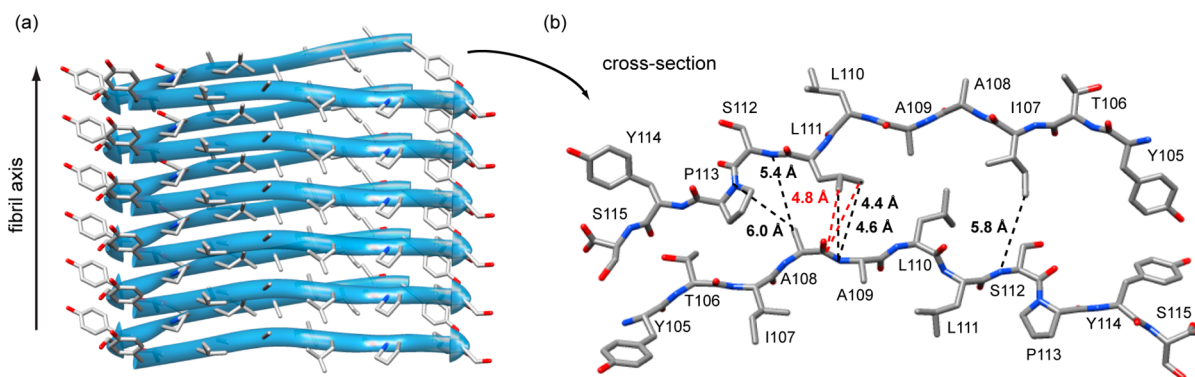


Figure 7. Structure of the TTR(105–115) protofilament (PDB ID: 2m5n, ref 30). (a) View along the fibril axis with an emphasis on the parallel, in-register β -strands within each β -sheet. (b) Summary of the observed quantitative contacts that constrain the odd–even–odd–even antiparallel β -sheet interface. Distances labeled in black were obtained with TEDOR, while the distances labeled in red were measured using R^2 TRW experiments. Images were produced with the Chimera software.⁷⁶

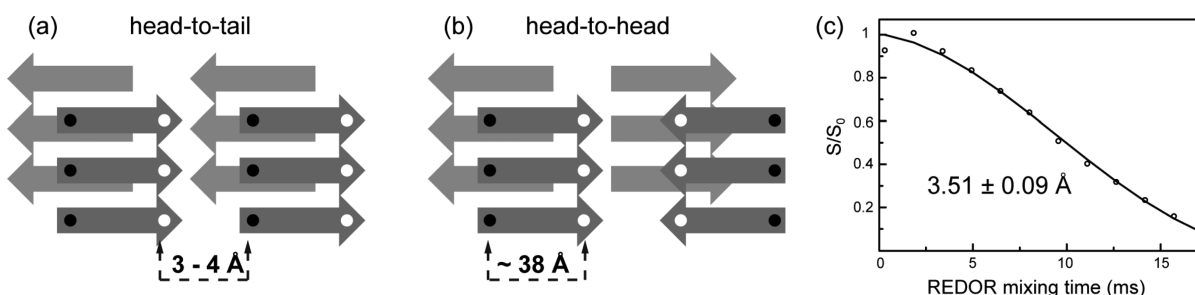


Figure 8. Two possible arrangements of the protofilaments are (a) head-to-tail and (b) head-to-head arrangements. Black circles correspond to a ^{15}N label in the N-terminus of the peptide, while the white circles represent the ^{13}C labeled carbonyl atom of the C-terminus, and the shortest expected ^{15}N – ^{13}C distances in each case are indicated. (c) A 1D DNP-enhanced ^{15}N – ^{13}C experiment recorded at a ^1H Larmor frequency of 400 MHz with REDOR mixing was used to measure the distance between the two labels. The fit distance is $3.51 \pm 0.09 \text{ \AA}$, consistent with a head-to-tail protofilament organization.

during these steps provides better resolution for the carbonyl region in the spectra. During the constant time mixing period that follows, polarization is transferred from the carbonyl atoms to the side chains via a combination of carefully selected spinning frequency and rf field strength. The spinning frequency $\omega_r/2\pi$ is selected such that $2 \times \omega_r/2\pi$ is slightly larger than the chemical shift difference in kHz between the carbonyls and the side-chain atoms of interest. The rf field strength applied during the mixing period is varied, adding a third dimension to the experiment. Figure 6b depicts two ^{15}N – ^{13}C correlations recorded with two different rf field strengths during mixing, showing several intramolecular cross peaks between the leucine carbonyl groups and side-chain atoms, as well as intermolecular cross peaks between A108CO and L111C δ 1 and C δ 2. The intensities of these cross peaks were fitted using a two-spin model as described in ref 73, and the best-fit distance for these two equivalent cross peaks was found to be $4.8 \pm 0.5 \text{ \AA}$.

Overall, 7 quantitative (ZF-TEDOR, R^2 TRW) and 16 semiquantitative ^{13}C – ^{13}C distances (PDSD) were used to define the intersheet interface, as described in detail in ref 30. The PAIN-CP experiments described here contributed two unique semiquantitative constraints (S112N–A108C α and I107N–P113C β). The cross peak between S112N and A108C α corresponds to a backbone-to-backbone intersheet contact of $\sim 7 \text{ \AA}$ based on the calculated structure. While such a distance is relatively long, it has been shown before, in model protein systems, that the TSAR mechanism can yield cross peaks for similar ^{15}N – ^{13}C distances under favorable spin

geometry.⁶⁸ Several other backbone-to-backbone intersheet correlations involving A108N might also be present in the PAIN-CP spectrum but they could not be assigned unambiguously due to the very similar chemical shifts of Y114N and A108N.

In order to satisfy the constraints required by all of the observed contacts (both quantitative and semiquantitative), the two sheets not only have to be arranged in an antiparallel manner with respect to each other but also need to possess a C2 symmetry with respect to an axis parallel to the intersheet direction. This requirement means that the side chains across the intersheet interface have to be arranged in an odd–even–odd–even manner (Figure 7b), similar to the class 4 peptide crystal interface described by Eisenberg and co-workers.³¹ Alternative arrangements including the odd–even–even–odd and the even–odd–odd–even arrangements were considered, but they do not satisfy the observed intersheet distance constraints (Figure S3).

Protofilament Arrangement. One of the most challenging aspects of studying the structure of amyloid fibrils is identifying the nature of the contacts between the protofilaments. In some cases, the ratio of the mass-per-length and the thickness of the fibril from cryo-EM data indicates that the fibril consists only of one protofilament (e.g., HET-s fibrils formed at pH > 3).^{77,78} In other amyloid systems (e.g., β_2 -microglobulin fibrils formed at pH 2.5), the cryo-EM density profile reveals a more complex arrangement with two sets of three different protofilaments arranged in a crescent shape.²³ In this case, different interfaces exist between protofilaments within each

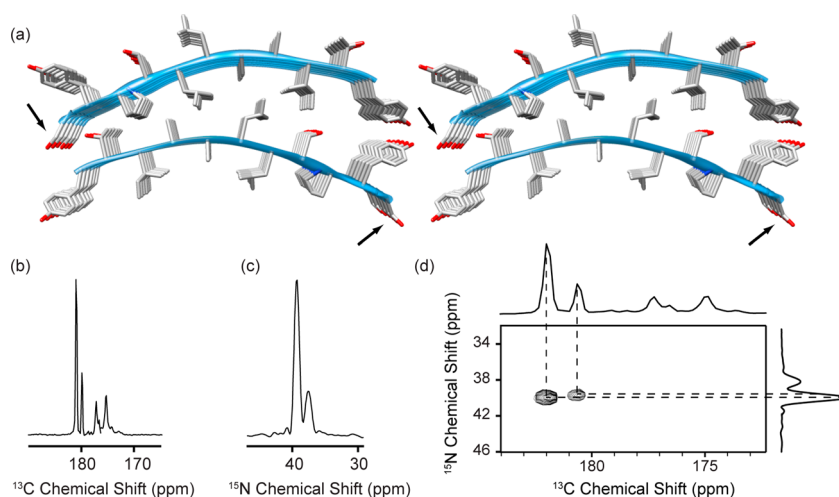


Figure 9. (a) Multiple peaks are observed in the spectra reflecting the four chemical environments expected for the termini in the TTR(105–115) fibrils (marked with arrows for the C-terminal case), PDB ID: 2m5k (ref 30). (b) ^{13}C MAS CP and (c) ^{15}N MAS CP spectra of a sample labeled with ^{13}C at the carbonyl S115 position and with ^{15}N at the Y105 position obtained at a ^1H Larmor frequency of 500 MHz. (d) TEDOR spectrum obtained with $\tau_{\text{mix}} = 8.5$ ms at the same field. The ^{13}C chemical shifts of the two cross peaks match the chemical shifts of the two major peaks in the 1D spectrum, while the average ^{15}N chemical shift of the cross peaks matches the chemical shift of the major ^{15}N peak.

creascent and between the two crescents. While obtaining distance constraints specific to the protofilament interface may be possible with MAS NMR (for an example involving $\text{A}\beta$ fibrils, see ref 79), information from other structural techniques is essential in doing so unambiguously.

The cryo-EM analysis of the TTR(105–115) fibrils identified three classes of fibrils, with cross-sectional widths of ~ 80 , ~ 120 , and ~ 160 Å, respectively.³⁰ The building block of the fibrils, as identified by NMR, consists of a pair of β -sheets, arranged in an antiparallel fashion, with an overall length of ~ 40 Å (Figure 7); this constitutes one protofilament in the fibrils. Based on the cryo-EM cross sections, there appear to be fibrils that consist of two, three, or four protofilaments. Since the fibrils are organized by stacking the building blocks laterally with respect to each other, one can then expect that the interactions between the protofilaments are between the termini of the peptides (Figure 8a,b). In this case, there are two possible arrangements: the C-terminus of a peptide from one protofilament faces the N-terminus of a peptide from the adjacent protofilament (“head-to-tail” arrangement), or the two peptides from adjacent protofilaments interact with each other through their C-termini or their N-termini only (“head-to-head” or “tail-to-tail” arrangement). These possibilities can be distinguished by placing a ^{15}N label on the N-terminus (Y105N) and a ^{13}C label on the C-terminus (S115C₁) of the peptide and measuring the distance between the labels.

Figure 8c shows a DNP-enhanced REDOR dephasing curve obtained for the S115 carbonyl peak. Fitting of the experimental data reveals that S115 C₁ is 3.51 ± 0.09 Å away from the only ^{15}N label in the sample (i.e., Y105N). This observation is consistent with the “head-to-tail” arrangement depicted in Figure 8a. Although the DNP data presented here were recorded with 256 scans per S and S_0 point (~ 5 h experimental time), sufficient signal-to-noise could have been obtained with fewer scans per point. An equivalent curve at room temperature with twice the amount of sample (15 mg) was recorded in ~ 1 day with a fit distance of 3.57 ± 0.06 Å.

Local Structural Variations in TTR(105–115) Fibrils.

The experiments described in the previous sections have allowed us to determine that the protofilament structure in the

TTR(105–115) fibrils consists of two parallel, in-register β -sheets forming an antiparallel odd–even–odd–even dry interface. This arrangement results in different chemical environments for the peptide residues as each side chain is exposed both to the dry β -sheet interface and to the solvent environments (Figure 9). Typically, such local structural variations are expected to generate two sets of chemical shifts in the NMR spectra. Furthermore, based on a DNP-enhanced REDOR experiment designed to detect ^{13}C – ^{15}N couplings between the peptide termini, we find that the protofilaments in the TTR(105–115) fibrils are arranged in a “head-to-tail” manner (Figure 8). Two additional local environments are then expected for the terminal sites of the peptide (Figure 9a) as the C-terminus of one peptide interacts with the N-terminus of a second peptide to form the protofilament-to-protofilament interface (“buried ends”), while the other ends of the two peptides face the solvent (“free ends”).

A careful analysis of the 2D correlation spectra presented above at different mixing times reveals that several residues do indeed display resolved peak multiplicities, including Y105 C α , S112 C α and C β , I107 C δ and C γ . The most striking examples of peak multiplicity, however, are found in the 1D spectra of the sample labeled with ^{13}C at the S115 carbonyl position only (C-terminus) and ^{15}N at the Y115 position only (N-terminus) (Figure 9b,c). The ^{13}C spectrum contains four peaks in the carbonyl region, while the ^{15}N spectrum contains two peaks with line widths that are larger than analogous signals of other residues. The observed peaks all have intensities well above the natural abundance background in the spectrum (Figure S4) and have been observed reproducibly in different sample preparations of the TTR(105–115) fibrils (Figure S5), including the identically labeled sample used in the DNP experiments (Figures 2 and 3b) and the YTIAALLSPYS labeled sample used for the TEDOR and PAINCP experiments.

Based on the “head-to-tail” protofilament-to-protofilament arrangement, only two of the ^{13}C peaks in Figure 9b should show REDOR dephasing since only two of the peptide ends participate in protofilament-to-protofilament interactions and are relatively close to the labeled nitrogen atom (3.5 Å) of the other protofilament (Figure 9a). The other two peaks are not

expected to show comparable dephasing as the average Ser115 $^{13}\text{C}'\text{--Tyr105 } ^{15}\text{N}$ distance across the sheet is $\sim 6 \text{ \AA}$ (PDB ID: 2m5n, ref 30). The REDOR data (Figure S6) do indeed reveal that two of the peaks (those with chemical shifts of 181.9 and 180.6 ppm) experience dephasing consistent with a $^{13}\text{C}\text{--}^{15}\text{N}$ distance of 3.5 \AA , and the other two peaks do not dephase significantly. In order to complement these REDOR data, we also recorded a 2D $^{15}\text{N}\text{--}^{13}\text{C}$ TEDOR correlation spectrum ($\tau_{\text{mix}} = 8.5 \text{ ms}$) that shows the same qualitative behavior (Figure 9d). The second dimension, however, also reveals that the two major ^{13}C peaks are correlated to two different ^{15}N atoms with chemical shifts that are $\sim 0.2 \text{ ppm}$ apart, indicating that there are two slightly different protofilament interfaces. These chemically inequivalent nitrogen environments cannot be resolved in the 1D spectrum in Figure 9c, and both fall under the intensity of the dominant ^{15}N peak in the spectrum. Their presence is, however, manifest in the relatively large line width of this peak (1 ppm, 50 Hz). Since the minor peak in the 1D spectrum presents similar line width (1.2 ppm, 60 Hz), it is likely to contain the contributions of the two expected “free” ^{15}N -labeled termini.

Different intensities are expected for the peaks corresponding to the “buried ends” versus the “free ends” as each sample contains a mixture of doublet, triplet, and quadruplet fibrils, as well as free protofilaments as described in ref 30. Since independent sample preparations might contain different ratios of these species, the total number of “buried” and “free” ends might vary from sample to sample, as evident in Figure S5. Further differences in intensity and line width might arise from differences in dynamics and local disorder potentially present at the four different sites.

The multiple peaks observed in the spectra of the terminal sites of the peptide are consistent with both the identified protofilament-to-protofilament interactions and the “odd–even–odd–even” β -sheet interface in the fibrils. The fact that two well-defined sets of cross peaks are not observed for the majority of the residues in the peptide is noteworthy and suggests that the local environments, particularly for the backbone atoms in the interior of the peptide, are not markedly different. Therefore, for most residues, the local structural variations imposed by the C2 symmetry of the structure remain hidden within the inhomogeneous line widths of the cross peaks.

CONCLUSIONS

In summary, we have presented MAS NMR experiments in conjunction with isotopic labeling schemes that have allowed us to characterize systematically the different levels of structural organization present in the amyloid fibrils formed by the 105–115 peptide segment of transthyretin. DNP-enhanced DQ-DRAWS and REDOR experiments performed at a ^1H Larmor frequency of 400 MHz with specifically labeled samples have allowed us to obtain high-quality data describing the β -strand and protofilament interactions within the fibrils in a fraction of the conventional experimental time. High-field, room temperature experiments performed at ^1H Larmor frequencies of 500, 750, and 900 MHz, on the other hand, have been essential in the unambiguous assignment and quantification of the long-range interactions that define the “odd–even–odd–even” β -sheet interface in the fibrils. The high-resolution nature of these experiments has also been crucial for identifying different conformations of both termini of the peptide molecules,

consistent with the manner in which the protofilaments are assembled into the fibril structure. Even at high-magnetic field, however, the differences in conformation that may be anticipated due to the “odd–even–odd–even” interface are not resolvable for many residues in the peptide molecule.

While our approach has relied on the use of site-specific labeling, which is more practical in synthetic peptides, the experimental principles described here have already been extended to amyloid systems formed by recombinantly produced proteins. For example, DNP-enhanced long-mixing ZF-TEDOR experiments together with samples prepared from a 50:50 mixture of ^{15}N and 2- ^{13}C glycerol labeled proteins have been used to define the parallel, in-register β -strand arrangement in fibrils formed by the 86-residue protein PI3-SH3.¹⁸ We envision that the availability of DNP/MAS NMR spectrometers operating at higher fields,^{80–82} together with amino acid specific, sparse, or segmentally labeled protein samples will provide the tools necessary to test hypotheses regarding the structural organization of larger amyloid systems in a more efficient manner.

The structure determination process described here was guided by information obtained via cryo-EM and X-ray diffraction that probe length scales larger than those accessible by NMR.³⁰ This information has allowed us to interpret the NMR data to define the multiple structural interactions that give rise to the remarkable stability of amyloid fibrils. The powerful combination of MAS NMR (with sensitivity enhancement provided from DNP) and such complementary methods will undoubtedly be widely applicable, leading to significant advances to our knowledge of the structure and properties of complex biological systems.

METHODS

Sample Preparation. Isotopically labeled amino acids were purchased from Cambridge Isotope Laboratories (Andover, MA), and solid-phase synthesis of the peptides was performed by CS Bio (Menlo Park, CA) and New England Peptide (Gardner, MA). Amyloid fibrils were prepared as previously described.³⁰ Briefly, the peptide was dissolved at a concentration of 15 mg/mL in 10% v/v acetonitrile/ H_2O (pH 2.0) and incubated at 37 $^\circ\text{C}$ for 2 days, followed by 14 days at 25 $^\circ\text{C}$. The resulting sample was transferred either into a 4 mm zirconia rotor (20 mg fibrils, Varian-Agilent Technologies, Santa Clara, CA) or a 3.2 mm zirconia rotor (15 mg of fibrils, Bruker BioSpin, Billerica, MA). We also recorded several spectra of a YTIAALLSPYS TTR(105–115) sample prepared from pure H_2O starting at 80 $^\circ\text{C}$ in order to increase the solubility of the peptide. The 1D and 2D spectra are identical to spectra of samples prepared from 10% acetonitrile/ H_2O solutions; a spectrum illustrating this point is shown in Figure S8.

DNP Experiments. The samples used for DNP were fibrilized following the procedure described above. After fibrilization, the samples were centrifuged at 320 000g for 2 h, and the pellets were resuspended in a solution containing a 60/40% w/w glycerol- d_8 /buffer matrix, where the buffer portion consisted of a 10/90% v/v acetonitrile/ D_2O mixture with pH adjusted to 2.0 with HCl. The matrix also contained 10 mM TOTAPOL.⁴⁰ The procedure was repeated with fresh buffer, and the resulting pellets were transferred into a 3.2 mm sapphire rotor ($\sim 8 \text{ mg}$ fibrils, Bruker BioSpin, Billerica, MA). The DNP experiments were performed on a Bruker 263 GHz Solids DNP spectrometer, consisting of a 263 GHz continuous-wave gyrotron source, microwave transmission line, 3.2 mm low temperature MAS probe, gas cooling supply, and 400 MHz AVANCE III wide-bore NMR system.⁸³ The DNP-enhanced DQ-DRAWS and REDOR experiments were performed at 100 K, $\omega_r/2\pi = 6.5 \text{ kHz}$ and a delay of 3 s between scans, and 55.5 kHz ^{13}C pulses and 40 kHz ^{15}N pulses were applied during the mixing periods of the experiments,

respectively. One hundred kilohertz TPPM⁸⁴ ^1H decoupling was used during acquisition and REDOR, while 100 kHz continuous-wave ^1H decoupling was applied during the DQ-DRAWS mixing period. The DNP-enhanced DQ-DRAWS experiment was recorded with 128 scans per mixing point, 14 mixing points, and overall acquisition time of ~ 1.5 h. The DNP-enhanced REDOR data were recorded with 256 scans per mixing point, 12 mixing points, and S and S_0 experiments were obtained. The overall time of this experiment was ~ 5 h.

Room Temperature MAS NMR Experiments. Two-dimensional PDS and PAIN-CP experiments were performed on a Bruker spectrometer operating at a ^1H Larmor frequency of 900 MHz, equipped with a triple-channel 3.2 mm E-free MAS probe (Bruker BioSpin, Billerica, MA). The sample used for these experiments was the uniformly ^{15}N , ^{13}C -labeled **YTIAALLSPYS**. The PDS experiments were performed at 11 kHz MAS and 83 kHz TPPM decoupling during acquisition. Thirty-two scans were recorded per t_1 point (892 t_1 points, 11.5 ms t_1 evolution, and 24 ms t_2 evolution). Experiments with $\tau_{\text{mix}} = 50, 100, 200,$ and 300 ms were collected. The PAIN-CP experiments were performed at 20 kHz MAS, while matching ~ 50 kHz ^1H B_1 field, ~ 50 kHz ^{13}C B_1 field, and ~ 35 kHz ^{15}N B_1 field during mixing. Sixty-four scans per t_1 point and 192 t_1 points were recorded, with 9.6 ms t_1 evolution, 18.4 ms t_2 evolution, and a scan delay of 2.7 s. Experiments with $\tau_{\text{mix}} = 4, 6, 8, 10,$ and 12 ms were collected. In these experiments, the center frequency was set to 40 ppm for ^{13}C and 126 ppm for ^{15}N .

ZF-TEDOR experiments were performed either on a custom-built spectrometer operating at 750 MHz ^1H Larmor frequency (**YTIAALLSPYS** sample) or on a spectrometer operating at 500 MHz (**YTIAALLSPYS** sample), both spectrometers courtesy of D. J. Ruben, Francis Bitter Magnet Laboratory, Massachusetts Institute of Technology, Cambridge, MA. For the **YTIAALLSPYS** sample, 40 kHz ^{15}N pulses, 83 kHz ^{13}C pulses, and 91 kHz ^1H TPPM decoupling during mixing and acquisition were used with $\omega_r/2\pi = 12.5$ kHz. One hundred twenty-eight scans per t_1 point and 256 t_1 points were collected, with 10.2 ms t_1 acquisition, 24 ms t_2 acquisition, and 2.7 s scan delay. Experiments with $\tau_{\text{mix}} = 4.8, 5.4, 6.0, 7.0, 7.6, 8.6, 9.6, 10.2, 11.8, 13.4,$ and 15 ms were collected. The ZF-TEDOR experiments with the **YTIAALLSPYS** sample were performed with 83 kHz ^1H TPPM decoupling, 83 kHz ^{13}C pulses, and 50 kHz ^{15}N pulses during mixing. R²TRW experiments were performed as described in ref 73, with 25 ms mixing, 83 kHz TPPM decoupling, and a carrier frequency set at 65 ppm and $\omega_r/2\pi = 10.1$ kHz. Spectra were indirectly referenced to DSS⁸⁵ and processed and analyzed using the programs NMRPipe⁸⁶ and Sparky.⁸⁷

Data Fitting. To extract quantitative distance information from DQ-DRAWS and TEDOR buildup curves and REDOR dephasing curves, we used the SPINEVOLUTION simulation program.⁶² The REDOR spectra were fitted according to the procedure detailed in ref 62. The DQ-DRAWS fit was based on four spins arranged in a square such that only the identical pairwise nearest-neighbor spin couplings were included in the simulation. This geometry gives rise to a periodic boundary condition that approximates well the infinite chain of labeled spins in the fibrils, while eliminating the effects of end spins on the simulation.⁶⁰ The error in the reported distances was based on the 95% confidence interval derived from the elements of the covariance matrix of the fit. In order to extract distances from TEDOR buildup curves, we approximated the Ala108 spin system by a ^{15}N atom and two ^{13}C atoms, corresponding to $C\alpha$ and $C\beta$, with $J_{C\alpha-C\beta} = 20$ Hz. For the simulation of longer distances, a second ^{15}N atom was included in the spin system, corresponding to Ile107N, Ser112N, or P113N. In this case, the distance between Ala108C β and the distant ^{15}N , in addition to a relaxation parameter, were used as fitting parameters in the simulations. The presence of the proximal ^{15}N (2.4 Å) was necessary for accurate simulation as it influences the long-distance TEDOR transfer dynamics quite significantly. The Ile107 spin system was approximated by a ^{15}N atom and four ^{13}C atoms (corresponding to $C\beta$, $C\gamma_2$, $C\gamma_1$, and $C\delta_1$). The J-coupling between $C\delta_1$ and $C\gamma_2$ was set to 20 Hz and was included in the simulation. Since there are no ^{15}N atoms within 4 Å from Ile107 C δ_1 , only one ^{15}N atom was

sufficient to describe the TEDOR transfer when fitting the Ile107N–C δ_1 and S112N–Ile107C δ_1 distances.

■ ASSOCIATED CONTENT

● Supporting Information

PAIN-CP buildup curves, additional TEDOR and REDOR data, alternative structural models of the intersheet interface, spectra of independent sample preparations. This material is available free of charge via the Internet at <http://pubs.acs.org>.

■ AUTHOR INFORMATION

Corresponding Author

rgg@mit.edu

Present Addresses

^{||}Department of Chemistry, Princeton University, Princeton, NJ 08544, U.S.A. (G.T.D.)

[■]Laboratory of Chemical Physics, National Institutes of Health, Bethesda, MD 20892, U.S.A. (M.J.B.)

[●]Physical Biology Center for Ultrafast Science and Technology, Arthur Amos Noyes Laboratory of Chemical Physics, California Institute of Technology, Pasadena, CA 91125, U.S.A. (A.W.F.)

[▼]Department of Physics, University of Guelph, Guelph, Ontario N1G 2W1, Canada (V.L.)

[◆]Department of Chemistry, Ohio State University, Columbus, OH 43210, U.S.A. (C.P.J.)

[▽]Department of Chemistry, UC Berkeley, 208C Stanley Hall, Berkeley, CA 94720–3220, U.S.A. (V.S.B.)

Notes

The authors declare no competing financial interest.

■ ACKNOWLEDGMENTS

We would like to thank Dr. David Ruben, Dr. Jochem Struppe, Dr. Shane Pawsey, Ajay Thakkar, and Leo Tometich for technical assistance and our colleagues Drs. Patrick van der Wel, Kendra Frederick, Vladimir Michaelis, Eugenio Daviso, Matthew Eddy, Loren Andreas, Helen Mott, Christopher Waudby, Alfonso De Simone, and Tuomas Knowles for many valuable discussions. We are grateful to Prof. Helen Saibil and Dr. Elena Orlova for providing the cryo-EM data (described in ref 30) and for their advice and comments. This work was supported by NIH grants EB-003151 and EB-002026, as well as by the UK BBSRC and the Wellcome and Leverhulme Trusts.

■ REFERENCES

- (1) Chiti, F.; Dobson, C. M. *Annu. Rev. Biochem.* **2006**, *75*, 333–366.
- (2) Fowler, D. M.; Koulov, A. V.; Balch, W. E.; Kelly, J. W. *TRENDS Biochem. Sci.* **2007**, *32*, 217–224.
- (3) Dobson, C. M. *Nature* **2003**, *426*, 884–890.
- (4) Nilsson, M. R. *Methods* **2004**, *34*, 151–160.
- (5) Sunde, M.; Serpell, L. C.; Bartlam, M.; Fraser, P. E.; Pepys, M. B.; Blake, C. C. F. *J. Mol. Biol.* **1997**, *273*, 729–739.
- (6) Comellas, G.; Rienstra, C. M. *Annu. Rev. Biophys.* **2013**, *42*, 515–536.
- (7) Petkova, A. T.; Yau, W. M.; Tycko, R. *Biochemistry* **2006**, *45*, 498–512.
- (8) Paravastu, A. K.; Leapman, R. D.; Yau, W. M.; Tycko, R. *Proc. Natl. Acad. Sci. U.S.A.* **2008**, *105*, 18349–18354.
- (9) Bertini, I.; Gonnelli, L.; Luchinat, C.; Mao, J.; Nesi, A. *J. Am. Chem. Soc.* **2011**, *133*, 16013–16022.
- (10) Wasmer, C.; Lange, A.; Van Melckebeke, H.; Siemer, A. B.; Riek, R.; Meier, B. H. *Science* **2008**, *319*, 1523–1526.

- (11) Van Melckebeke, H.; Wasmer, C.; Lange, A.; Eiso, A. B.; Loquet, A.; Bockmann, A.; Meier, B. H. *J. Am. Chem. Soc.* **2010**, *132*, 13765–13775.
- (12) Heise, H.; Hoyer, W.; Becker, S.; Andronesi, O. C.; Riedel, D.; Baldus, M. *Proc. Natl. Acad. Sci. U.S.A.* **2005**, *102*, 15871–15876.
- (13) Vilar, M.; Chou, H. T.; Luhrs, T.; Maji, S. K.; Riek-Loher, D.; Verel, R.; Manning, G.; Stahlberg, H.; Riek, R. *Proc. Natl. Acad. Sci. U.S.A.* **2008**, *105*, 8637–8642.
- (14) Comellas, G.; Lemkau, L. R.; Nieuwkoop, A. J.; Kloepper, K. D.; Ladrer, D. T.; Ebusu, R.; Woods, W. S.; Lipton, A. S.; George, J. M.; Rienstra, C. M. *J. Mol. Biol.* **2011**, *411*, 881–895.
- (15) Debelouchina, G. T.; Platt, G. W.; Bayro, M. J.; Radford, S. E.; Griffin, R. G. *J. Am. Chem. Soc.* **2010**, *132*, 10414–10423.
- (16) Debelouchina, G. T.; Platt, G. W.; Bayro, M. J.; Radford, S. E.; Griffin, R. G. *J. Am. Chem. Soc.* **2010**, *132*, 17077–17079.
- (17) Bayro, M. J.; Maly, T.; Birkett, N. R.; MacPhee, C. E.; Dobson, C. M.; Griffin, R. G. *Biochemistry* **2010**, *49*, 7474–7484.
- (18) Bayro, M. J.; Debelouchina, G. T.; Eddy, M. T.; Birkett, N. R.; MacPhee, C. E.; Rosay, M.; Maas, W. E.; Dobson, C. M.; Griffin, R. G. *J. Am. Chem. Soc.* **2011**, *133*, 13967–13974.
- (19) Helmus, J. J.; Surewicz, K.; Nadaud, P. S.; Surewicz, W. K.; Jaroniec, C. P. *Proc. Natl. Acad. Sci. U.S.A.* **2008**, *105*, 6284–6289.
- (20) Helmus, J. J.; Surewicz, K.; Apostol, M. I.; Surewicz, W. K.; Jaroniec, C. P. *J. Am. Chem. Soc.* **2011**, *133*, 13934–13937.
- (21) Jimenez, J. L.; Guijarro, J. L.; Orlova, E.; Zurdo, J.; Dobson, C. M.; Sunde, M.; Saibil, H. R. *EMBO J.* **1999**, *18*, 815–821.
- (22) Zhang, S.; Andreasen, M.; Nielsen, J. T.; Liu, L.; Nielsen, E. H.; Song, J.; Ji, G.; Sun, F.; Skrydstrup, T.; Besenbacher, F.; Nielsen, N. C.; Otzen, D. E.; Dong, M. *Proc. Natl. Acad. Sci. U.S.A.* **2013**, *110*, 2798–2803.
- (23) White, H. E.; Hodgkinson, J. L.; Jahn, T. R.; Cohen-Krausz, S.; Gosal, W. S.; Muller, S.; Orlova, E. V.; Radford, S. E.; Saibil, H. R. *J. Mol. Biol.* **2009**, *389*, 48–57.
- (24) Sachse, C.; Fandrich, M.; Grigorieff, N. *Proc. Natl. Acad. Sci. U.S.A.* **2008**, *105*, 7462–7466.
- (25) Wegmann, S.; Medalsy, I. D.; Mandelkow, E.; Müller, D. J. *Proc. Natl. Acad. Sci. U.S.A.* **2012**, *110*, E313–E321.
- (26) Blake, C. C. F.; Geisow, M. J.; Oatley, S. J.; Rerat, B.; Rerat, C. J. *Mol. Biol.* **1978**, *121*, 339–356.
- (27) Gustavsson, A.; Engstrom, U.; Westermark, P. *Biochem. Biophys. Res. Commun.* **1991**, *175*, 1159–1164.
- (28) Jaroniec, C. P.; MacPhee, C. E.; Astrof, N. S.; Dobson, C. M.; Griffin, R. G. *Proc. Natl. Acad. Sci. U.S.A.* **2002**, *99*, 16748–16753.
- (29) Jaroniec, C. P.; MacPhee, C. E.; Bajaj, V. S.; McMahon, M. T.; Dobson, C. M.; Griffin, R. G. *Proc. Natl. Acad. Sci. U.S.A.* **2004**, *101*, 711–716.
- (30) Fitzpatrick, A. W. P.; Debelouchina, G. T.; Bayro, M. J.; Clare, D. K.; Caporini, M. A.; Bajaj, V. S.; Jaroniec, C. P.; Wang, L.; Ladizhansky, V.; Müller, S.; Aaj, MacPhee, C. E.; Waudby, C. A.; Mott, H. R.; De Simone, A.; Knowles, T. P. J.; Saibil, H. R.; Vendruscolo, M.; Orlova, E. V.; Griffin, R. G.; Dobson, C. M. *Proc. Natl. Acad. Sci. U.S.A.* **2013**, *110*, 5468–5473.
- (31) Sawaya, M. R.; Sambashivan, S.; Nelson, R.; Ivanova, M. I.; Sievers, S. A.; Apostol, M. I.; Thompson, M. J.; Balbirnie, M.; Wiltzius, J. J. W.; McFarlane, H. T.; Madsen, A. O.; Riek, C.; Eisenberg, D. *Nature* **2007**, *447*, 453–457.
- (32) Kessenikh, A. V.; Lushchikov, V. I.; Manenkov, A. A.; Taran, Y. V. *Sov. Phys.—Solid State* **1963**, *5*, 321–329.
- (33) Hwang, C. F.; Hill, D. A. *Phys. Rev. Lett.* **1967**, *18*, 110–112.
- (34) Goldman, M. *Spin temperature and nuclear magnetic resonance in solids*; Clarendon Press: Oxford, U.K., 1970.
- (35) Atsarkin, V. A. *Sov. Phys. Usp.* **1978**, *21*, 725–744.
- (36) Abragam, A.; Goldman, M. *Nuclear magnetism: order and disorder*; Clarendon Press: Oxford, U.K., 1982.
- (37) Becerra, L. R.; Gerfen, G. J.; Temkin, R. J.; Singel, D. J.; Griffin, R. G. *Phys. Rev. Lett.* **1993**, *71*, 3561–3564.
- (38) Hall, D. A.; Maus, D. C.; Gerfen, G. J.; Inati, S. J.; Becerra, L. R.; Dahlquist, F. W.; Griffin, R. G. *Science* **1997**, *276*, 930–932.
- (39) Maly, T.; Debelouchina, G. T.; Bajaj, V. S.; Hu, K.-N.; Joo, C.-G.; Mak-Jurkauskas, M. L.; Sirigiri, J. R.; van der Wel, P. C. A.; Herzfeld, J.; Temkin, R. J.; Griffin, R. G. *J. Chem. Phys.* **2008**, *128*, 052211.
- (40) Song, C.; Hu, K. N.; Joo, C. G.; Swager, T. M.; Griffin, R. G. *J. Am. Chem. Soc.* **2006**, *128*, 11385–11390.
- (41) Mak-Jurkauskas, M. L.; Bajaj, V. S.; Hornstein, M. K.; Belenky, M.; Griffin, R. G.; Herzfeld, J. *Proc. Natl. Acad. Sci. U.S.A.* **2008**, *105*, 883–888.
- (42) Bajaj, V. S.; Mak-Jurkauskas, M. L.; Belenky, M.; Herzfeld, J.; Griffin, R. G. *Proc. Natl. Acad. Sci. U.S.A.* **2009**, *106*, 9244–9249.
- (43) Goncalves, J. A.; Ahuja, S.; Erfani, S.; Eilers, M.; Smith, S. O. *Prog. Nucl. Magn. Reson. Spectrosc.* **2010**, *57*, 159–180.
- (44) Linden, A. H.; Lange, S.; Franks, W. T.; Akbey, Ü.; Specker, E.; van Rossum, B.-J.; Oshkinat, H. *J. Am. Chem. Soc.* **2011**, *133*, 19266–19269.
- (45) Reggie, L.; Lopez, J. J.; Collinson, I.; Glaubitz, C.; Lorch, M. *J. Am. Chem. Soc.* **2011**, *133*, 19084–19086.
- (46) Andreas, L. B.; Barnes, A. B.; Corzilius, B. R.; Chou, J. J.; Miller, E. A.; Caporini, M.; Rosay, M.; Griffin, R. G. *Biochemistry* **2013**, *52*, 2774–2782.
- (47) van der Wel, P. C. A.; Hu, K. N.; Lewandowski, J.; Griffin, R. G. *J. Am. Chem. Soc.* **2006**, *128*, 10840–10846.
- (48) Debelouchina, G. T.; Bayro, M. J.; van der Wel, P. C. A.; Caporini, M. A.; Barnes, A. B.; Rosay, M.; Maas, W. E.; Griffin, R. G. *Phys. Chem. Chem. Phys.* **2010**, *12*, 5911–5919.
- (49) Takahashi, H.; Ayala, I.; Bardet, M.; De Paepe, G.; Simorre, J.-P.; Hediger, S. *J. Am. Chem. Soc.* **2013**, *135*, 5105–5110.
- (50) Renault, M.; Pawsey, S.; Bos, M. P.; Koers, E. J.; Nand, D.; Tommassen-van Boxtel, R.; Rosay, M.; Tommassen, J.; Maas, W. E.; Baldus, M. *Angew. Chem., Int. Ed.* **2012**, *51*, 2998–3001.
- (51) Jaroniec, C. P.; Filip, C.; Griffin, R. G. *J. Am. Chem. Soc.* **2002**, *124*, 10728–10742.
- (52) Petkova, A. T.; Ishii, Y.; Balbach, J. J.; Antzutkin, O. N.; Leapman, R. D.; Delaglio, F.; Tycko, R. *Proc. Natl. Acad. Sci. U.S.A.* **2002**, *99*, 16742–16747.
- (53) Luca, S.; Yau, W. M.; Leapman, R.; Tycko, R. *Biochemistry* **2007**, *46*, 13505–13522.
- (54) Iwata, K.; Fujiwara, T.; Matsuki, Y.; Akutsu, H.; Takahashi, S.; Naiki, H.; Goto, Y. *Proc. Natl. Acad. Sci. U.S.A.* **2006**, *103*, 18119–18124.
- (55) Kryndushkin, D. S.; Wickner, R. B.; Tycko, R. *J. Mol. Biol.* **2011**, *409*, 263–277.
- (56) Nelson, R.; Sawaya, M. R.; Balbirnie, M.; Madsen, A. O.; Riek, C.; Grothe, R.; Eisenberg, D. *Nature* **2005**, *435*, 773–778.
- (57) Tycko, R. *J. Chem. Phys.* **2007**, *126*, 064506.
- (58) Benzinger, T. L. S.; Gregory, D. M.; Burkoth, T. S.; Miller-Auer, H.; Lynn, D. G.; Botto, R. E.; Meredith, S. C. *Proc. Natl. Acad. Sci. U.S.A.* **1998**, *95*, 13407–13412.
- (59) Karlsson, T.; Popham, J. M.; Long, J. R.; Oyler, N.; Drobny, G. P. *J. Am. Chem. Soc.* **2003**, *125*, 7394–7407.
- (60) Caporini, M. A.; Bajaj, V. S.; Veshtort, M.; Fitzpatrick, A.; MacPhee, C. E.; Vendruscolo, M.; Dobson, C. M.; Griffin, R. G. *J. Phys. Chem. B* **2010**, *114*, 13555–13561.
- (61) Chang, J. J.; Griffin, R. G.; Pines, A. *J. Chem. Phys.* **1975**, *62*, 4923–4926.
- (62) Veshtort, M.; Griffin, R. G. *J. Magn. Reson.* **2006**, *178*, 248–282.
- (63) van der Wel, P. C. A.; Lewandowski, J. R.; Griffin, R. G. *J. Am. Chem. Soc.* **2007**, *129*, 5117–5130.
- (64) van der Wel, P. C. A.; Lewandowski, J.; Griffin, R. G. *Biochemistry* **2010**, *44*, 9457–9469.
- (65) Nielsen, J. T.; Bjerring, M.; Jeppesen, M. D.; Pedersen, R. O.; Pedersen, J. M.; Hein, K. L.; Vosegaard, T.; Skrydstrup, T.; Otzen, D. E.; Nielsen, N. C. *Angew. Chem., Int. Ed.* **2009**, *48*, 2118–2121.
- (66) Szeverenyi, N. M.; Sullivan, M. J.; Maciel, G. E. *J. Magn. Reson.* **1982**, *47*, 462–475.
- (67) Lewandowski, J. R.; De Paepe, G.; Griffin, R. G. *J. Am. Chem. Soc.* **2007**, *129*, 728–729.

- (68) De Paepe, G.; Lewandowski, J. R.; Loquet, A.; Eddy, M.; Megy, S.; Bockmann, A.; Griffin, R. G. *J. Chem. Phys.* **2011**, *134*, 095101.
- (69) Veshkort, M.; Griffin, R. G. *J. Chem. Phys.* **2011**, *135*, 134509.
- (70) Nieuwkoop, A. J.; Wylie, B. J.; Franks, W. T.; Shah, G. J.; Rienstra, C. M. *J. Chem. Phys.* **2009**, *131*, 095101.
- (71) Bayro, M. J.; Huber, M.; Ramachandran, R.; Davenport, T. C.; Meier, B. H.; Ernst, M.; Griffin, R. G. *J. Chem. Phys.* **2009**, *130*, 114506.
- (72) De Paepe, G.; Lewandowski, J. R.; Loquet, A.; Bockmann, A.; Griffin, R. G. *J. Chem. Phys.* **2008**, *129*, 245101.
- (73) Ladizhansky, V.; Griffin, R. G. *J. Am. Chem. Soc.* **2004**, *126*, 948–958.
- (74) Pines, A.; Gibby, M. G.; Waugh, J. S. *J. Chem. Phys.* **1972**, *56*, 1776.
- (75) Baldus, M.; Petkova, A. T.; Herzfeld, J.; Griffin, R. G. *Mol. Phys.* **1998**, *95*, 1197–1207.
- (76) Pettersen, E. F.; Goddard, T. D.; Huang, C. C.; Couch, G. S.; Greenblatt, D. M.; Meng, E. C.; Ferrin, T. E. *J. Comput. Chem.* **2004**, *25*, 1605–1612.
- (77) Sen, A.; Baxa, U.; Simon, M. N.; Wall, J. S.; Sabate, R.; Saupe, S. J.; Steven, A. C. *J. Biol. Chem.* **2007**, *282*, 5545–5550.
- (78) Mizuno, N.; Baxa, U.; Steven, A. C. *Proc. Natl. Acad. Sci. U.S.A.* **2011**, *108*, 3252–3257.
- (79) Agarwal, V.; Linser, R.; Dasari, M.; Fink, U.; del Amo, J.-M. L.; Reif, B. *Phys. Chem. Chem. Phys.* **2013**, *15*, 12551–12557.
- (80) Matsuki, Y.; Ueda, K.; Idehara, T.; Ikeda, R.; Ogawa, I.; Nakamura, S.; Toda, M.; Anai, T.; Fujiwara, T. *J. Magn. Reson.* **2012**, *225*, 1–9.
- (81) Pike, K. J.; Kemp, T. F.; Takahashi, H.; Day, R.; Howes, A. P.; Kryukov, E. V.; MacDonald, J. F.; Collis, A. E. C.; Bolton, D. R.; Wylde, R. J.; Orwick, M.; Kosuga, K.; Clark, A. J.; Idehara, T.; Watts, A.; Smith, G. M.; Newton, M. E.; Dupree, R.; Smith, M. E. *J. Magn. Reson.* **2012**, *215*, 1–9.
- (82) Barnes, A. B.; Markhasin, E.; Daviso, E.; Michaelis, V. K.; Nanni, E. A.; Jawa, S. K.; Mena, E. L.; DeRocher, R.; Thakkar, A.; Woskov, P. P.; Herzfeld, J.; Temkin, R. J.; Griffin, R. G. *J. Magn. Reson.* **2012**, *224*, 1–7.
- (83) Rosay, M.; Tometich, L.; Pawsey, S.; Bader, R.; Schauwecker, R.; Blank, M.; Borchard, P. M.; Cauffman, S. R.; Felch, K. L.; Weber, R. T.; Temkin, R. J.; Griffin, R. G.; Maas, W. E. *Phys. Chem. Chem. Phys.* **2010**, *12*, 5850–5860.
- (84) Bennett, A. E.; Rienstra, C. M.; Auger, M.; Lakshmi, K. V.; Griffin, R. G. *J. Chem. Phys.* **1995**, *103*, 6951–6958.
- (85) Morcombe, C. R.; Zilm, K. W. *J. Magn. Reson.* **2003**, *162*, 479–486.
- (86) Delaglio, F.; Grzesiek, S.; Vuister, G. W.; Zhu, G.; Pfeifer, J.; Bax, A. *J. Biomol. NMR* **1995**, *6*, 277–293.
- (87) Goddard, T. D.; Kneller, D. G. *Sparky 3*. University of California, San Francisco, 2008.